Heliyon 9 (2023) e22536

Contents lists available at ScienceDirect

Heliyon

journal homepage: www.cell.com/heliyon

Research article

Brain tumor feature extraction and edge enhancement algorithm based on U-Net network

Dapeng Cheng [a,b,*], Xiaolian Gao [a], Yanyan Mao [a], Baozhen Xiao [c], Panlu You [a], Jiale Gai [a], Minghui Zhu [a], Jialong Kang [d], Feng Zhao [a,b], Ning Mao [e]

[a] School of Computer Science and Technology, Shandong Business and Technology University, No.191 Binhai Middle Road, Yantai City, Shandong Province, Yantai, 264000, China

[b] Shandong Co-Innovation Center of Future Intelligent Computing, No.191 Binhai Middle Road, Yantai City, Shandong Province, Yantai, 264000, China

[c] Early Spring Garden Primary School, 6452 Fushou East Street, Weifang City, Shandong Province, Weifang, 261000, China

[d] School of Information and Electronic Engineering, Shandong Business and Technology University, No.191 Binhai Middle Road, Yantai City, Shandong Province, Yantai, 264000, China

[e] Department of Radiology, Yantai Yuhuangding Hospital, No.20, Yudong Road, Yantai City, Shandong Province, Yantai, 264000, China

ARTICLE INFO

Dataset link: https://doi.org/10.1016/j.compbiomed.2019.05.002

Dataset link: https://doi.org/10.6084/m9.figshare.1512427.v5

Dataset link: https://doi.org/10.48550/arXiv.2107.02314

Keywords:
U-Net
VGG-19
Attention mechanism
Edge detection

ABSTRACT

Background: Statistics show that each year more than 100,000 patients pass away from brain tumors. Due to the diverse morphology, hazy boundaries, or unbalanced categories of medical data lesions, segmentation prediction of brain tumors has significant challenges.

Purpose: In this thesis, we highlight EAV-UNet, a system designed to accurately detect lesion regions. Optimizing feature extraction, utilizing automatic segmentation techniques to detect anomalous regions, and strengthening the structure. We prioritize the segmentation problem of lesion regions, especially in cases where the margins of the tumor are more hazy.

Methods: The VGG-19 network structure is incorporated into the coding stage of the U-Net, resulting in a deeper network structure, and an attention mechanism module is introduced to augment the feature information. Additionally, an edge detection module is added to the encoder to extract edge information in the image, which is then passed to the decoder to aid in reconstructing the original image. Our method uses the VGG-19 in place of the U-Net encoder. To strengthen feature details, we integrate a CBAM (Channel and Spatial Attention Mechanism) module into the decoder to enhance it. To extract vital edge details from the data, we incorporate an edge recognition section into the encoder.

Results: All evaluation metrics show major improvements with our recommended EAV-UNet technique, which is based on a thorough analysis of experimental data. Specifically, for low contrast and blurry lesion edge images, the EAV-Unet method consistently produces forecasts that are very similar to the initial images. This technique reduced the Hausdorff distance to 1.82, achieved an F1 score of 96.1%, and attained a precision of 93.2% on Dataset 1. It obtained an F1 score of 76.8%, a Precision of 85.3%, and a Hausdorff distance reduction to 1.31 on Dataset 2. Dataset 3 displayed a Hausdorff distance cut in 2.30, an F1 score of 86.9%, and Precision of 95.3%.

Conclusions: We conducted extensive segmentation experiments using various datasets related to brain tumors. We refined the network architecture by employing smaller convolutional kernels in

* Corresponding author at: School of Computer Science and Technology, Shandong Business and Technology University, Yantai, China.
E-mail address: chengdapeng@sdtbu.edu.cn (D. Cheng).

https://doi.org/10.1016/j.heliyon.2023.e22536
Received 14 June 2023; Received in revised form 2 November 2023; Accepted 14 November 2023

Available online 21 November 2023
2405-8440/© 2023 The Author(s). Published by Elsevier Ltd. This is an open access article under the CC BY-NC-ND license (http://creativecommons.org/licenses/by-nc-nd/4.0/).

our strategy. To further improve segmentation accuracy, we integrated attention modules and an edge enhancement module to reinforce edge information and boost attention scores.

1. Introduction

In the realm of neurological conditions, brain lesions stand out as a significant pathological entity. The World Health Organization (WHO) reports that there are about 260,000 cases of brain cancer worldwide each year. Remarkably, brain tumors rank among the leading causes of death in developed countries. If not provided with appropriate medical intervention, this condition may result in severe outcomes, such as visual impairment, speech impairment, and sometimes even paralysis. In medical image analysis, accurately identifying and classifying brain tumors is a critical task for clinical diagnosis, developing treatment plans, and tracking the course of the disease. The arrival of automated segmentation techniques has greatly advanced the understanding of medical professionals regarding tumor volumetric properties and space distribution. This development has therefore made it easier to provide more accurate and customized medical treatments. Nevertheless, it is crucial to emphasize the inherent complexities involved in distinguishing the boundaries between normal tissues that surround pathological tumor areas.

Conventional methods for segmenting imaging data have depended on human experts feature extraction and threshold setting, introducing intrinsic obstacles in capturing the complex features of tumor boundaries. In recent times, the field of medical segmentation has witnessed notable advancements in performance, owing to the substantial contributions of deep learning techniques. These cutting-edge approaches have become essential instruments for conducting thorough case analyses and research projects, which have resulted in ground-breaking discoveries. Ongoing study and development are necessary to further investigate and enhance the refinement of marginal information within the domain of brain tumor segmentation.

(1) Picture Quality: Inherent factors like noise, artifacts, and variations in scanning parameters can impair the clarity of CT scans and MRI. These factors reduce edge-based precision, which makes it difficult for the model to identify tumorous regions spatially, as shown graphically in Fig. 1.

(2) Structural Ambiguity: Determining the exact borders of tumors poses a challenge owing to the subtle features of the brain's soft tissue. As seen graphically in Fig. 2, these intricacies result in hazy lesion borders, which create morphological variances and size uncertainties among various kinds of brain tumors.

(3) Annotation Inclination: Manual annotations require the subjective assessment of individual experts, potentially resulting in biased labels. Previous research suggests that this kind of bias in annotations during training can have a significant impact on segmentation algorithms' performance [1].

(4) Data imbalance: A notable category imbalance is a fundamental issue with medical datasets, which can cause a bias in favor of categories with large sample counts during training. For instance, in cases where the oedema region is disproportionately represented in comparison to the tumor region, the learning model may potentially amplify the morphological characteristics of the oedema, resulting in misclassification of the oedema as tumor tissue. [2–4]

A higher degree of complexity is present in the segmentation of brain tumors in the clinical setting [5]. The goal of this work is to examine the effectiveness of different approaches in obtaining accurate tumor edge data. We provide an improved U-Net variation, called EAV-UNet, whose goal is to maximize target picture feature discrimination. An edge detection module that is specially tuned to lesion borders is incorporated into the segmentation network framework to handle problems (1) and (2). This combination leverages the complementary strengths of attention processes and convolutional neural networks to enable the reliable and sophisticated extraction of complex tumor edge information. During the encoding phase, we leverage the large perceptual field that the convolutional layers provide to improve the extraction of subtle picture information, which increases the sensitivity of edge detection. We use the Focal Tversky Loss function, which has been carefully tuned to reduce problems with data imbalance by modifying hyperparameters, for difficulties (3) and (4). Through thorough experimentation, we systematically evaluate this model's performance advantages over traditional approaches in brain tumor segmentation with the goal of promoting the adoption of more accurate and effective clinical techniques.

The significance of precision in image processing is emphasized in the existing body of literature. The utilization of stacked hybrid blocks including different kernel sizes presents a flexible and adaptable approach that can effectively meet a wide range of needs. The RepLKNet architecture, which incorporates a wide convolutional kernel, was introduced by Ding et al. [6]This design innovation incorporates sophisticated methodologies such as structural reparameterization and complicated deep convolutional layers. Consequently, there is a heightened acquisition of worldwide characteristics, significantly augmenting the accuracy of brain tumor identification in imaging investigations. Zong et al. [7] conducted a prominent study that emphasized the effectiveness of mega-convolution in the context of specific image datasets. The study showcased the model's impressive performance, achieving a top-1 accuracy of 87.8% and a mIoU measure of 56% on the ADE20K dataset. With the goal to reach global information capture, Zhou et al. [8] conducted an assessment of four pooling approaches and devised two strategies, namely "variable" and "invariant", to enhance the scope of sensory fields. Ding et al. [9] incorporated the principles of ACNet into the underlying framework of VGG in the RepVGG design. The objective of this merger was to tackle the difficulties related to the training accuracy of VGG [10], while still retaining the advantages of using small convolutional kernels. This approach prioritized the capture of local information. In contrast to ResNet50 [11], a harmonious balance between accuracy and runtime speed was achieved, registering a top-1 accuracy

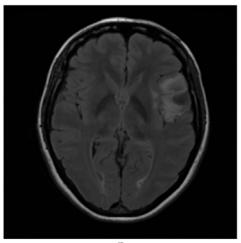

Fig. 1. This picture shows a low-grade glioma from a low-contrast MRI.

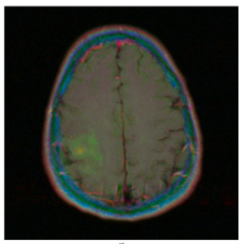

Fig. 2. This MRI shows an unclearly marginated low-grade glioma.

exceeding 80% on the ImageNet dataset and realizing an enhancement in runtime speed to 83%. As the network layers become more complex, the challenges of gradient explosion and vanishing become critical to address. Deshpande et al. [12] employed ResNet for distinguishing brain tumor types, accomplishing super-resolution, and further evolving the concept by extending residual links to encompass dense connections.

The investigation conducted by Zhou et al. [13] explored several GAN network, emphasizing their significance within the domain of medical image fusion, a critical component in the diagnosis of medical diseases. The segmentation impact is influenced by the clarity of the image. Argus et al. [14] highlighted the capability of MRI (magnetic resonance imaging) to acquire high-resolution pictures by the manipulation of the surrounding tissue in the region of interest [15,16]. In a subsequent study, Zhao et al. [17] integrated the UNet [18] with full convolutional networks (FCN) [19] to create a novel segmentation approach. They also introduced a partially constructed codec as part of their end-to-end solution. The RMCA U-Net was developed by incorporating unique adaptations to the traditional U-Net framework in a later improvement [20]. The present iteration employed a residual technique in conjunction with a channel attention mechanism, so establishing a foundation for intricate retinal diagnosis pertaining to diabetes. R et al. [21] proposed the utilization of reversible blocks as a means to alleviate memory constraints and facilitate the storage of activation functions. Hao et al. [22] presented a novel approach NPC for segmenting using a combination of pixel edge and region-level collaborative loss. Li et al. [23] proposed an innovative method aimed at improving the clarity of focus information in medical pictures, with the ultimate goal of achieving more precise lesion segmentation. In addition, the ANU-Net, which incorporates attention gates into the skip connections of the U-Net, represents a considerable advancement in the field. Furthermore, Zhou et al. [24] made modifications to the jump connection inside the U-Net architecture and built a novel network called UNet++. This modification involves aggregating data from several layers through feature stacking, hence enhancing the model's representation capabilities. The UNet++ architecture incorporates a deeply supervised network approach, which leverages intermediate monitoring signals to streamline the training process.

Medical images possess inherent characteristics that result in concerns of privacy, imbalanced data distribution, and uncertainty in the morphology of lesions. Moreover, the complexity of neural network topologies amplifies the susceptibility of medical data. The utilization of multi-task learning paradigms has been shown to effectively leverage latent knowledge [25–27]. Woo et al. [28] combine spatial and channel attention techniques in order to enhance important characteristics. It's noteworthy to mention that the delineation of adjacent tissue plays a consequential role in influencing segmentation precision. In order to tackle this issue, Shen et al. [29] proposed an edge detection module that effectively disseminates information via an encoder. In continuation of this research trajectory, Sun et al. [30] introduced the AS-UNet model to address the difficulties associated with segmenting lesion edges. They enhanced their model by incorporating edge feature mapping in the decoding phase. Although these investigations have provided useful insights, the complexities associated with brain tumor segmentation continue to be an ongoing problem. Brain tumors exhibit complex shapes, low MRI contrast, diverse tissue properties, and ill-defined edges, all of which hinder the accuracy of training. This study aims to enhance the U-Net framework by deepening the network structure using small convolutional kernels. Through meticulous analysis of experimental parameters, we propose the integration of the CBAM attention mechanism module in the decoding phase to optimize the scoring of critical feature information and extract more valuable insights. An edge enhancement module is incorporated during the encoding stage to mitigate information gaps within regions and accentuate lesion edge contours.

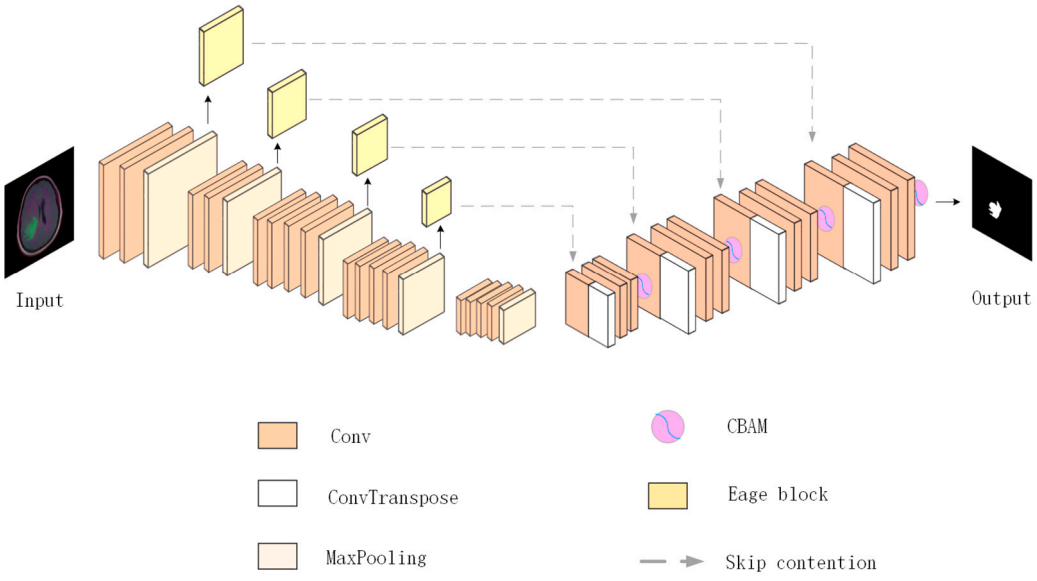

Fig. 3. The EAV-UNet network follows a structured architectural design.

2. Materials and methods

2.1. Network structure

The article presents the introduction of a novel medical image segmentation network called EAV-UNet. EAV-UNet is an improved version of the U-Net design, as illustrated in Fig. 3. Its architecture comprises three key components: an edge detection convolutional layer (E), an attention mechanism (A), and a deepening VGG19 network structure (V). In this study, we employ the encoding-decoding structure of the U-Net, with the encoding part replaced by the VGG19 network to significantly deepen the network layers and extract feature information at a profound level. The utilization of jump connections allows the transfer of feature information extracted from higher layers to lower layers within the network. Notably, the feature maps of each layer in the encoding are channeled into the edge detection convolution module, leading to the generation of edge feature maps. These edge feature maps, acting as an additional source of edge details, are conveyed to the corresponding decoder layers at the same hierarchical level via jump connections. Additionally, we introduce the CBAM attention mechanism module into the decoder path to refine the output results. To address data imbalances in brain tumor images, we incorporate the Focal Tversky loss function into the training model. This addition serves to reduce classification complexity and enhance lesion prediction accuracy.

2.2. Fusion of VGG19 and U-Net

The encoder is to obtain high-level features from the input medical picture, which are subsequently utilized by the decoder modules for generating predictions or segmenting the image. In practice, additional computational tasks are often integrated to enhance segmentation predictions. However, this augmentation increases the model's complexity. Consequently, some researchers prefer the utilization of 3x3 convolutional kernels over larger counterparts, aiming to mitigate parameter and computational overhead. This preference is particularly relevant for network architectures handling multi-channel datasets. The employment of multiple smaller convolutional kernels offers several advantages. Firstly, it reduces the number of activation layers, emphasizing the nonlinear representations within the model. Secondly, it enhances information capture through diverse feature extraction. In our proposed model, we leverage the VGG19 architecture for the encoder. This strategic choice deepens the network's architecture and enhances the efficiency of information extraction. Furthermore, to augment the model's generalization capacity and overall robustness, the encoder leverages pre-trained weights derived from the VGG19 network.

While U-Net has demonstrated effectiveness in small-sample image segmentation, it exhibits limitations in capturing intricate features. In contrast, VGG19 employs a multi-layer architecture designed for progressive feature extraction, particularly well-suited for large-scale image categorization or segmentation. Given the strong feature extraction performance of the U-Net's encoding module, which bears structural resemblance to VGG-19, we have chosen to replace the U-Net encoder with VGG19 while preserving the fundamental U-Net framework. Our evaluation metrics reveal a notable 5.3% improvement in the accuracy of the predicted images.

2.3. Attention mechanism module

When processing feature maps with an excessive number of image features, computers may produce outputs that lack focus and are inadequate in representing the target region. The attention mechanism in computer vision seeks to identify correlations among the

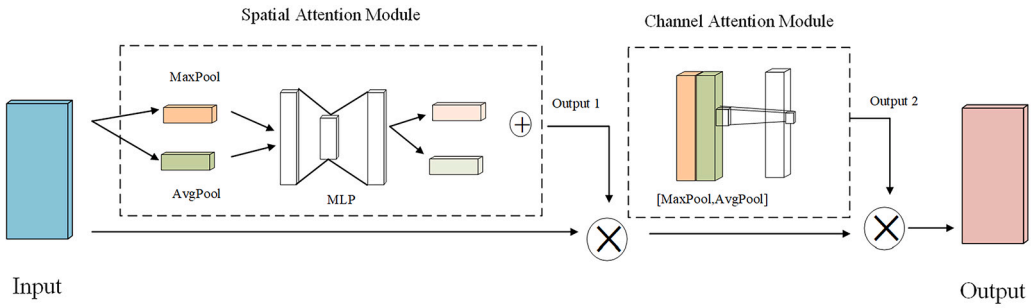

Fig. 4. CBAM structure diagram.

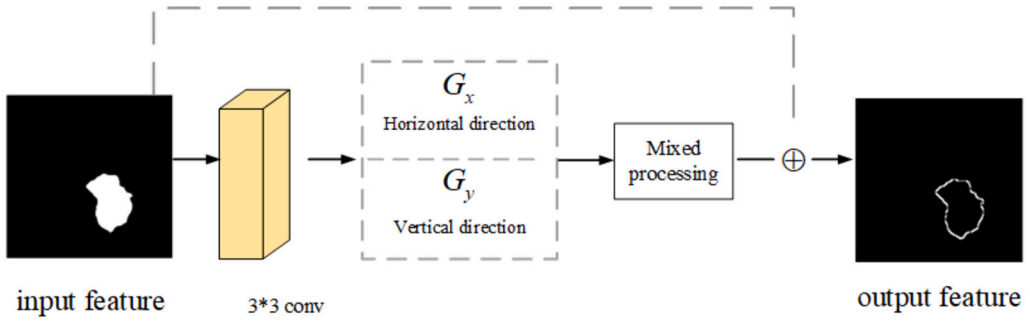

Fig. 5. Structure of the edge enhancement module.

original data while highlighting important features. This paper introduces the Convolutional Block Attention Module (CBAM [28]) in decoder stage. During the encoding step, the feature information is passed through the channel (CA) and spatial (SA) attention mechanism consecutively. The former focuses on the content of the feature information, while the latter emphasizes the location of the feature information. The configuration of the CBAM is illustrated in Fig. 4.

The feature map outputted by the convolutional layer initially enters the channel attention module, where the feature map is compressed into a one-dimensional vector along the spatial dimension. Following maximum pooling and average pooling, it is fed into the shared neural network (MLP). The resulting feature maps are element-wise summed and merged after expanding along the spatial dimension, yielding output1. The resulting feature map, denoted as channel attention feature map, is obtained by multiplying output1 with the input feature map. Subsequently, the result is input into the SA module, undergoing maximum pooling and average pooling, which are then concatenated into a feature map. After applying a 7x7 convolutional kernel for dimensionality reduction, output2 is obtained. Finally, the generated feature is acquired by the process of multiplying the created feature with the initial input feature map, denoted as “Input”.

In this paper, our model employs both the CA and SA mechanism sequentially to extract meaningful and relevant features, thereby enhancing the model’s training accuracy. This enables the model to disregard irrelevant noise information and concentrate on extracting key information.

2.4. Convolutional layer for edge detection

The most significant challenge in medical image processing is accurately delineating lesion edges. Due to the variable shapes of tumor borders and the relatively smooth nature of surrounding tissues, models often struggle to capture edge details, resulting in inaccurate segmentation outcomes. To tackle this challenge, this paper introduces an edge detection convolutional layer after each layer in the encoding stage of the model, effectively utilizing the Sobel operator [31] for image edge detection, as depicted in Fig. 5. The Sobel operator employs a 3x3 convolution kernel containing two matrices, S_x and S_y. A grayscale weighting algorithm is applied to the 3x3 neighborhood around each pixel to compute gradient values in both horizontal and vertical directions. These gradients are then combined and processed, as described in equation (3), to emphasize edge points, leading to enhanced edge detection. The resultant edge detection feature maps are subsequently integrated into the decoder stage through jump connections. The convolution factors S_x and S_y of the Sobel operator are defined in equation (1).

$$S_x = \begin{bmatrix} -1 & 0 & 1 \\ -2 & 0 & 2 \\ -1 & 0 & 1 \end{bmatrix}, S_y = \begin{bmatrix} 1 & 2 & 1 \\ 0 & 0 & 0 \\ -1 & -2 & -1 \end{bmatrix} \tag{1}$$

I represents the original image, where G_x, G_y represent the gradients in the vertical and horizontal directions, as illustrated in equation (2).

$$G_x = S_x \times I, G_y = S_y \times I \tag{2}$$

The grayscale values of each pixel in both the vertical and horizontal axes are combined.

$$G = \sqrt{{G_x}^2 + {G_y}^2} \tag{3}$$

2.5. Focal Tversky loss function

The commonly used loss function in image processing, known as the generalized cross-entropy loss (GCE) [32], is computed on a per-pixel basis. However, the field of medical imaging frequently encounters the obstacle of data imbalance. Data imbalances can lead to a biased class-led learning process, making it difficult for classes with fewer pixels to extract meaningful features. Additionally, in medical images, the small regions of interest (ROIs) in lesions often lead to heavily biased high-precision but low-recall predictions, which can diminish the model's effectiveness. To address the issue of significant classification errors caused by the disproportion of positive and negative samples during training, we focus our attention on samples with limited data. We incorporate a hyperparameter, denoted as 'α', into the Tversky Loss function [33], which is a modified version of the binary cross-entropy loss, as shown in equation (4).

$$Tversky = \frac{\sum_{i=1}^{N} p_{ic} o_{ic} + s}{\sum_{i=1}^{N} p_{ic} o_{ic} + \alpha \sum_{i=1}^{N} p_{ic} o_{i\overline{c}} + (1-\alpha) \sum_{i=1}^{N} p_{i\overline{c}} o_{ic} + s} \tag{4}$$

Where p_{ic} is the probability that pixel i is predicted to belong to category c, $p_{i\overline{c}}$ is the probability that pixel i is predicted to belong to category c, o_{ic} is the probability that pixel i actually belongs to category c, $o_{i\overline{c}}$ is the probability that pixel i actually belongs to category c, α is a hyperparameter that shifts the focus of attention by adjusting the hyperparameter, and s is a constant that provides data stability. Tversky loss actually solves the issue pertaining to samples that are positive or negative, and we further realize the distinction between difficult samples. By intervening with the hyperparameter β, the Focal Tversky loss function [34] improves the classification difficulty of samples on lesion training and achieves a better balance between accuracy and recall, as in equation (5). The Focal Tversky Loss function was assigned the value of $\alpha = 0.7$, $\beta = 0.75$ based on empirical investigation.

$$FT = \sum_{c} (1 - Tversky)^{\beta} \tag{5}$$

3. Results

3.1. Data sets

In this study, the model has been trained using three distinct datasets to assess its generalization and robustness.

Dataset 1: The data used in our experiments were sourced from The Cancer Genome Atlas (TCGA) [35], where brain tumor images from 110 patients with low-grade gliomas were identified, collected from five different institutions. Specifically, we utilized the LGG Segmentation Dataset, compiled as described by Mateusz et al. [36]. This dataset comprises open low-grade glioma MRI scans, encompassing both normal brain images and brain tumor images. Our experimental dataset consisted of 2556 images without brain tumors and 1373 images with brain tumors. To ensure a robust evaluation, the dataset was partitioned into 22 distinct subsets that were mutually exclusive, each containing images from 5 different patients selected from the total of 110 patients. These subsets were further divided into testing, validation, and training sets, with 1167 images allocated to the training set and 103 images each for the testing and validation sets.

Dataset 2: The dataset employed in this article, referred to as the 'brain tumor dataset', was obtained from Figshare and was originally made available by Jun Cheng [37]. This dataset comprised a total of 3064 T1-weighted pictures, which were representative of three distinct categories of brain tumors. Initially provided in MAT file format, we employed a custom data processing script to convert it into a more suitable numpy array format for deep learning models. This preprocessing involved tasks such as loading the MAT files, resizing all images to a consistent 256x256 pixel dimensions, and randomly partitioning the dataset into three subsets, accounting for 70%, 15% and 15% respectively. This approach ensures both dataset uniformity and randomness. Finally, the partitioned dataset was saved as a numpy array file, making it easily accessible for future research.

Dataset 3: The dataset utilized in this study consists of images sourced from the BraTS 2021 training set, which is part of the BraTS Challenge [38]. This dataset comprises a total of 1251 cases and includes MRI images of the brain captured from various axial perspectives. To facilitate model training, we extracted 2D image slices from each axial view, specifically the transverse, coronal, and sagittal views. These image slices were further processed to categorize the data from various imaging modalities into binary categories before being utilized as input data for model training.

3.2. Evaluation indicators and experimental details

The experiments detailed in this paper were conducted using a Windows operating system, Python 3.7 programming language, and the Keras 2.4.3 deep learning framework with a TensorFlow 2.4.0 backend. Furthermore, the experiments made use of a configuration featuring a CUDA 11.5 RTX 3060Ti graphics card and the CUDNN 8.0 deep neural network model training library. Throughout the model training process, several key parameters were employed. The initial rate of learning was established as 0.01, the batch size

was specified as 6. The Adam optimizer was utilized with an epsilon value of 0.1. Additionally, a maximum of 200 iterations were specified for each training run.

In this paper, we use Focal Tversky index (FT), Precision (Pre), Intersection over Union (IoU), F1 Score (F1), Structural Similarity Index (SSIM), Hausdorff Distance (HD) and Mean Absolute Error (MAE) as evaluation indicators to measure the prediction results of the model and make a more scientific evaluation. Among them, precision focuses on the accuracy of the model prediction results and is particularly suitable for measuring sample imbalance problems like medical image processing; IoU evaluated the segmentation capacity of the model; The F1 measure is responsible for adjusting the weights of Precision (Pre) and Recall (R) in various scenarios; The Structural Similarity Index (SSIM) is a metric used to quantify the degree of resemblance between an image and its original structure, encompassing attributes such as brightness and contrast; The Hausdorff Distance (HD) is employed to quantify the discrepancy at the boundary of the designated region; the Mean Absolute Error (MAE) is utilized to assess the average absolute difference between the anticipated outcome and the initial image. The evaluation metrics are calculated as shown in equations (6), (7), (8), (9), (10).

$$\mathrm{Pre} = \frac{TP}{TP + FP} \tag{6}$$

$$R = \frac{TP}{TP + FN}, F1 = \frac{2 \times Pre \times R}{Pre + R} \tag{7}$$

where TP is a True positive case, TN is a True negative case, FP is a False positive case, and FN is a False negative case.

$$SSIM(x, y) = \frac{(2\mu_x\mu_y + C_1)(2\sigma_{xy} + C_2)}{(\mu_x{}^2 + \mu_y{}^2 + C_1)(\sigma_x{}^2 + \sigma_y{}^2 + C_2)} \tag{8}$$

where μ_x, μ_y denote the brightness of the original image and the predicted image respectively, σ_x, σ_y denote the contrast of the original image and the predicted image respectively, and C_1, C_2 is a constant.

$$HD = H(A, B) = \max\left[h(A, B), h(B, A)\right] \tag{9}$$

Where H is the Hausdorff function, A is the prediction result, B is the original image, $A = \{a_1, a_2, \cdots\}$, $B = \{b_1, b_2, \cdots\}$ is the two-point set, $h(A, B) = \max_{a \in A} \min_{b \in B} \|a - b\|$, $h(B, A) = \max_{a \in A} \min_{b \in B} \|b - a\|$, $H(A, B)$ is the Hausdorff bidirectional distance, the unidirectional Hausdorff distance (HD) from point set A to point set B is denoted as $h(A, B)$, while the unidirectional Hausdorff distance (HD) from point set B to point set A is denoted as $h(B, A)$.

$$MAE = \frac{1}{m}\sum_{i=1}^{m}\left|B_i - A_i\right| \tag{10}$$

Where m represents the total number of samples, B_i denotes the original image, A_i signifies the prediction result, and the function $|\cdot|$ stands for the absolute value computation.

3.3. Ablation experiments

The efficacy of the suggested model was validated through the implementation of ablation experiments in this research. These studies encompass the following key enhancements: (1) Integration of U-Net with VGG-19: This augmentation deepens the network structure while significantly enhancing the capacity for feature information extraction, despite the increase in parameter count. (2) Introduction of CBAM Attention Mechanism: Within the decoding stage, the CBAM attention mechanism is incorporated. It involves the processing of output feature maps from all layers, employing both channel attention (CA) and spatial attention (SA) modules. When compared to the baseline U-Net, this modification leads to an improvement in accuracy: 8% on Dataset 1, 3.6% on Dataset 2, and 0.2% on Dataset 3. Additionally, it results in a reduction in the Mean Absolute Error (MAE) by 0.46% and 0.14% on Dataset 1 and 2, respectively, as well as 0.81% on Dataset 3, underscoring the effectiveness of the enhanced attention mechanism.(3) Incorporation of Edge Detection Convolutional Layer: An edge detection convolutional layer is introduced into each encoder layer to enhance the precision of lesion edge detection. This enhancement yields superior outcomes, particularly in relation to the Hausdorff distance (HD) metric, achieving optimal scores of 1.82, 1.31, and 2.30, respectively. These enhancements have been seamlessly integrated into our model's architecture and their feasibility for enhancing model performance has been rigorously demonstrated through experimental data, as presented in Table 1.

3.4. Comparative experiments

This study involved the implementation of comparative experiments on three separate datasets in order to assess the efficacy of different convolutional neural network designs for medical image segmentation. Specifically, we investigated the Full Convolutional Neural Network (FCN), the U-Net network, and two modified approaches based on the U-Net framework. FCN and U-Net are well-established segmentation networks widely used within the domain of medical image analysis. We also investigated UNet++, a novel architecture that enhances the U-Net framework by incorporating a pruning mechanism and deep supervision techniques to improve overall model performance. Additionally, we introduced AS-UNet, an innovative variant of U-Net. AS-UNet integrates an

Table 1
Comparison of various functional modules and overall network structures in different brain tumor image segmentation tasks.

Dataset	model	Pre	IoU	F1	SSIM	HD	MAE (%)	FT
Dataset 1	U-Net	0.843	0.856	0.922	0.881	10.4	0.67%	0.83
	+VGG19	0.882	0.875	0.903	0.954	8.50	0.37%	0.88
	+CBAM	0.923	0.791	0.883	0.967	4.12	0.21%	0.86
	+Edge	0.918	0.897	0.936	0.934	2.83	0.34%	0.88
	EAV-UNet	0.932	0.924	0.961	0.968	1.82	0.18%	0.93
Dataset 2	U-Net	0.782	0.778	0.717	0.918	2.38	4.19%	0.76
	+VGG19	0.815	0.815	0.732	0.930	2.21	3.82%	0.82
	+CBAM	0.818	0.803	0.719	0.926	2.15	4.05%	0.75
	+Edge	0.932	0.812	0.722	0.931	2.03	3.18%	0.82
	EAV-Unet	0.853	0.842	0.768	0.931	1.31	2.85%	0.83
Dataset 3	U-Net	0.919	0.779	0.876	0.905	8	1.64%	0.82
	+VGG19	0.923	0.830	0.892	0.895	5.82	0.62%	0.88
	+CBAM	0.921	0.812	0.831	0.926	6.31	0.83%	0.73
	+Edge	0.928	0.822	0.826	0.902	4.28	1.58%	0.77
	EAV-Unet	0.953	0.831	0.869	0.958	2.3	1.02%	0.85

Table 2
EAV-UNet was compared with the baseline U-Net model and three other relevant network models for image segmentation across various brain tumor datasets.

Datasets	model	Pre	IoU	F1	SSIM	HD	MAE(%)	FT
Dataset 1	FCN	0.831	0.795	0.886	0.903	11.3	0.60%	0.75
	U-Net	0.843	0.856	0.922	0.881	10.4	0.67%	0.83
	UNet++	0.862	0.835	0.820	0.921	11.4	1.09%	0.82
	AS-Unet	0.891	0.846	0.917	0.967	3.24	0.76%	0.82
	EAV-Unet	0.932	0.924	0.961	0.968	1.82	0.18%	0.93
Dataset 2	FCN	0.671	0.625	0.552	0.843	13.8	6.35%	0.64
	U-Net	0.782	0.778	0.717	0.918	2.38	4.19%	0.76
	UNet++	0.735	0.652	0.685	0.921	4.23	5.12%	0.71
	AS-Unet	0.831	0.805	0.683	0.926	1.82	4.32%	0.80
	EAV-Unet	0.853	0.842	0.768	0.931	1.31	2.85%	0.83
Dataset 3	FCN	0.791	0.658	0.812	0.759	23.8	9.36%	0.69
	U-Net	0.919	0.779	0.876	0.905	8.00	1.64%	0.82
	UNet++	0.896	0.832	0.854	0.892	6.76	1.98%	0.79
	AS-Unet	0.932	0.815	0.882	0.912	6.32	2.47%	0.83
	EAV-Unet	0.953	0.831	0.869	0.958	2.30	1.02%	0.85

Edge-Attention module within the last three layers of the U-Net decoder. This module is specifically devised to tackle the difficulties related to the segmentation of picture edges.

The experimental findings, as presented in Table 2, demonstrate the greater efficacy of our proposed approach in comparison to four alternative methodologies. Despite the relatively simpler architectures of FCN and U-Net networks, which result in fewer parameters, our method excels comprehensively across all evaluation metrics. Specifically, on Dataset 2, our method demonstrates substantial improvements, with Precision (Pre) metrics surpassing those of FCN and U-Net by 16% and 7.1%, respectively. Furthermore, in comparison to UNet++, our method on Dataset 1 achieves a 5.9% increase in Precision (Pre) and a 2.7% enhancement in the F1 score, while simultaneously reducing the mean absolute error (MAE) by 0.91%. These findings underscore the superior feature information extraction capabilities during the encoding phase, in contrast to the decoding phase. Moreover, when compared with AS-UNet, our method yields significant improvements in Hausdorff distance metrics, with reductions of 1.42, 12.49, and 5.7 on the respective datasets. This observation indicates enhanced proficiency in edge identification, hence reinforcing the efficacy of our approach.

Visualizations were obtained from various methods applied to three distinct datasets, each comprising the original brain tumor image, its corresponding Ground Truth, and the predicted segmentation outcomes generated by different network architectures. The figures presented depict the red contour, which serves to show the extracted original mask area, while the green region represents the segmented tumor.

Fig. 6 and Fig. 7 display the image results obtained from Dataset 1. A detailed analysis of these images reveals the following observations: FCN exhibits subpar predictive performance, particularly when confronted with images characterized by low contrast. It struggles to accurately delineate and segment lesion regions. UNet++, on the other hand, demonstrates less effective predictions, especially when dealing with images featuring boundary smoothing and blurring characteristics. In comparison, the AS-UNet model excels in terms of its similarity to the original image and its ability to capture information related to lesion edges and blurred images. However, it slightly lags behind the method proposed in this paper in certain aspects. EAV-UNet's prediction results closely

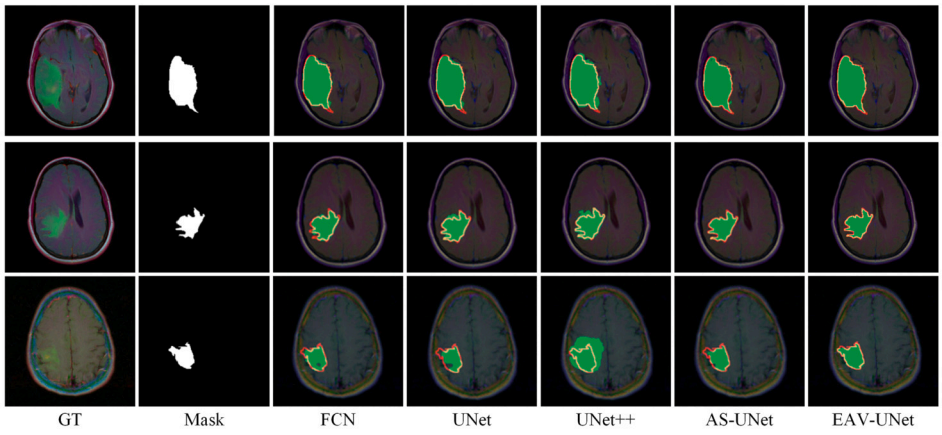

Fig. 6. Visualization results of EAV-UNet and four other methods in the high-contrast image segmentation task of the LGG Segmentation Dataset.

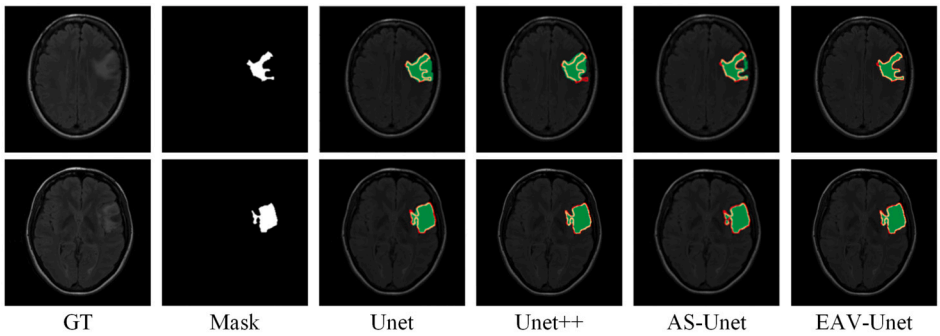

Fig. 7. Visualization results of EAV-UNet and four other methods in the low-contrast image segmentation task of the LGG Segmentation Dataset.

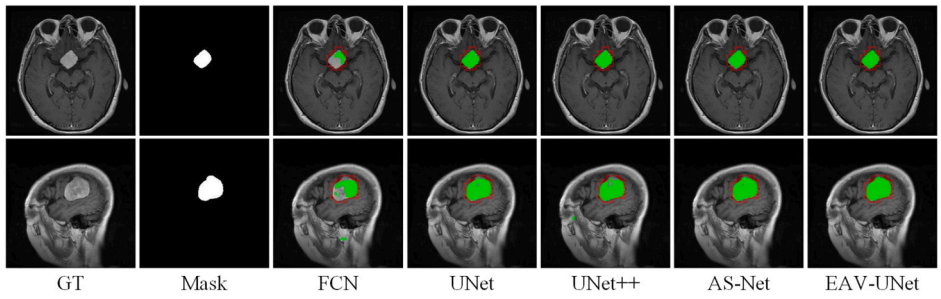

Fig. 8. Visualization results of EAV-UNet and other network models in the brain tumor Dataset segmentation task.

align with the original images, especially when dealing with images featuring complex lesion edges and low contrast. It effectively highlights lesion regions and, as a result, achieves the highest level of accuracy among the evaluated models. Fig. 8 presents the visualization results obtained from Dataset 2, also known as the Brain Tumor Dataset. This dataset encompasses various brain tumor types, each characterized by diverse shapes, textures, and boundary features. The presence of such data diversity significantly contributes to enhanced model training, enabling it to effectively adapt to these inherent variations. Notably, the incorporation of T1-weighted contrast-enhanced pictures serves to emphasize the boundaries of brain tumors and other discernible characteristics, hence facilitating accurate identification and segmentation of the tumors. When we compare the network model incorporating edge enhancement with the original U-Net and FCN models, a clear emphasis on the lesion's edge region becomes evident in the visualization results. Upon closer scrutiny, it becomes apparent that EAV-UNet excels in generating predictions that closely resemble the original images, particularly when handling complex boundary scenarios. The visualization results presented in Fig. 9 are obtained from Dataset 3. BraTS2021 dataset is a comprehensive collection that includes four distinct imaging modalities, effectively covering a wide range of brain tumor types. This dataset provides a rich and diverse set of data, which plays a crucial role in enhancing our model's ability to comprehend intricate information. Traditional methodologies and alternative deep learning models may encounter performance limitations due to inherent challenges such as boundary ambiguities and regional inhomogeneities, which further complicate the task of precise segmentation. However, by adopting the EAV-UNet method, we have successfully overcome these

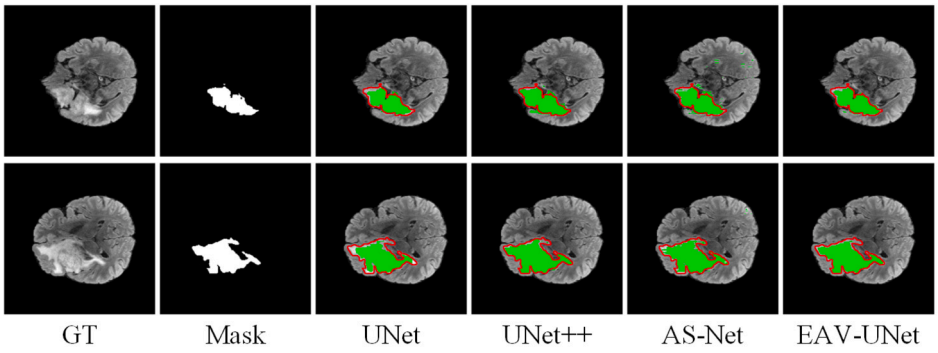

Fig. 9. Visualized results of EAV-UNet and other network models in the BraTS2021 segmentation task.

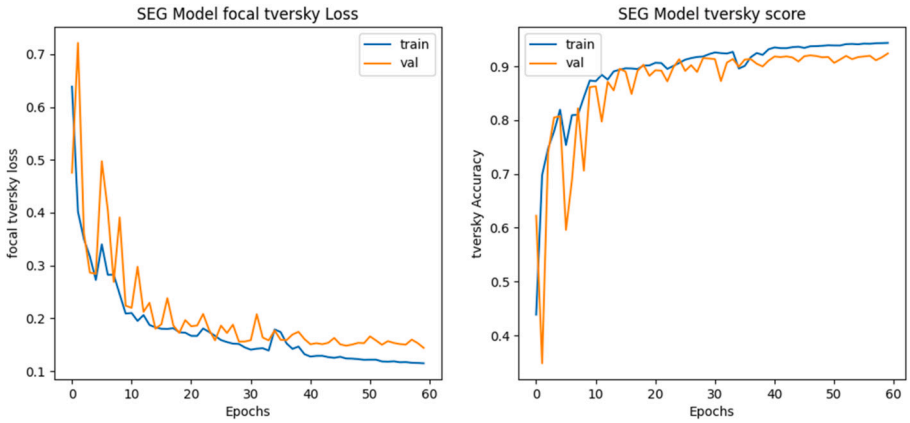

Fig. 10. Optimal hyperparameters set at $\alpha = 0.7, \beta = 0.75$ for loss function analysis. The left panel presents the model's training progression via the Focus Tversky loss, while the right panel showcases the training evolution in terms of the Tversky index.

Table 3
Experimental results of Focal Tversky loss with different hyperparameters.

α ($\beta = 0.75$)	0.9	0.7	0.5	0.3	0.1
Loss	0.341	0.144	0.173	0.153	0.176
Score	0.659	0.856	0.827	0.847	0.694

challenges, thereby demonstrating the efficacy of our methodology in attaining superior segmentation results in the context of brain tumor analysis.

3.5. Experimental results of Focal Tversky loss with different hyperparameters

To optimize performance, we make adjustments to parameters α, β achieving the optimal configuration. Fig. 10 displays the loss function for hyperparameters $\alpha = 0.7$ and $\beta = 0.75$. Fig. 11 illustrates the results of the Focal Tversky loss function for our method with different hyperparameters α. Compared with Fig. 11. (a),(b),(c),(d), it becomes evident that the loss is minimized when $\alpha = 0.7$ and $\beta = 0.75$. The curve presented in Fig. 11. (b) or the validation set aligns better with the test set, but results in higher loss values. However, apart from Fig. 11 (b), the other three plots exhibit noticeable oscillations, and the losses do not yield favorable results, can be explained to the discrepancy between the chosen loss function and the hyperparameter. Specific experimental data are provided in Table 3 for further analysis.

4. Discussion

The article presents a novel brain tumor segmentation technique, referred to as EAV-UNet, with a primary focus on edge enhancement. Drawing upon insights from contemporary deep learning network models and benchmarking against other methods, we strategically leverage the VGG19 architecture. Our approach involves the replacement of the U-Net network structure with smaller convolutional and pooling kernels, resulting in a reduction of network parameters and an enhancement in the capture of detailed

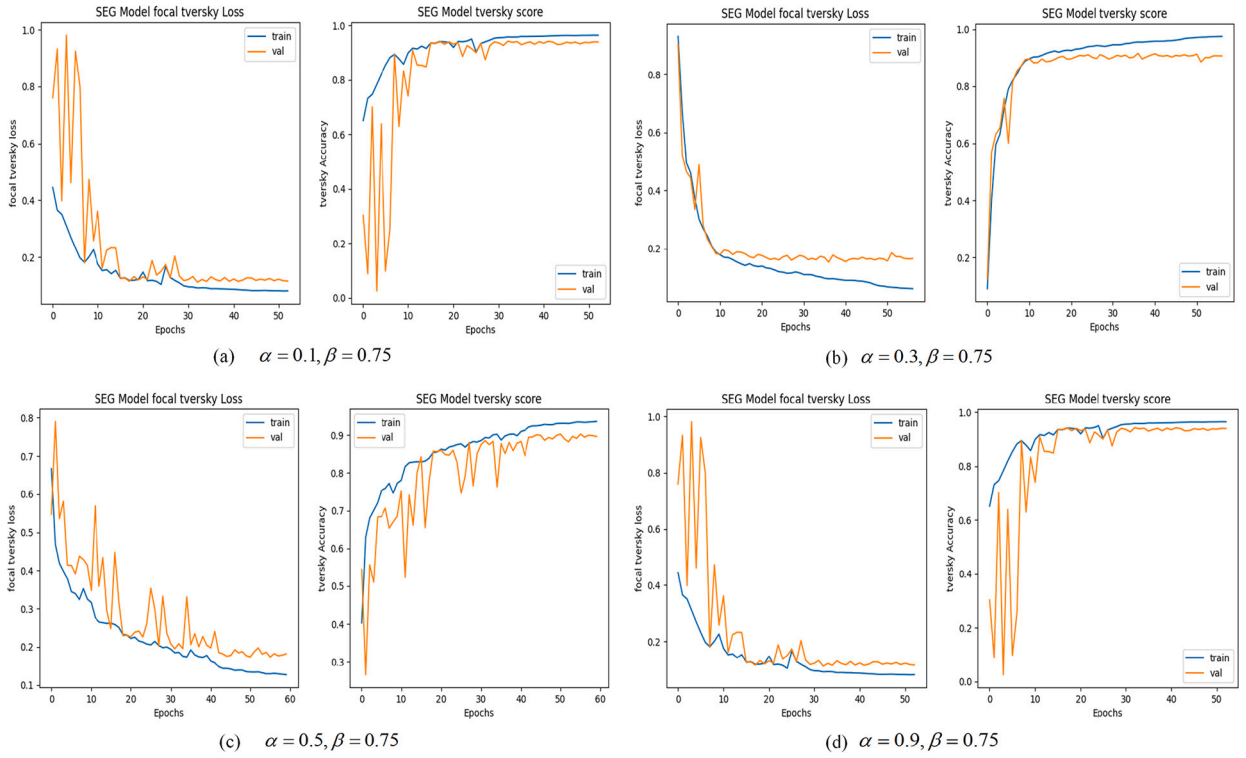

Fig. 11. Training results for Focal Tversky loss under various hyperparameters. Panel (a) displays the model's training loss curve (left) and Tversky index progression (right) with hyperparameter set at '$\alpha = 0.1, \beta = 0.75$'. Similarly, panels (b), (c), and (d) depict the training trajectories under the hyperparameter settings '$\alpha = 0.3, \beta = 0.75$', '$\alpha = 0.5, \beta = 0.75$', and '$\alpha = 0.9, \beta = 0.75$' respectively. The left side of each panel presents the associated loss curve, while the right side illustrates the Tversky index curve.

information within the feature graph. This refinement proves particularly advantageous for large-scale datasets, especially those encompassing a substantial volume of medical images, as empirically demonstrated in our experiments.

Our method undergoes extensive validation across three distinct datasets: the LGG Segmentation Dataset, brain tumor dataset, and BraTS2021. Diverging from conventional brain tumor segmentation techniques, our primary focus centers on the precise delineation of tumor edge information an essential element for preoperative assessment and treatment planning. Through the integration of scoring mechanisms, we augment edge features, effectively addressing common challenges related to edge blurring and indistinct segmentation within brain tumor segmentation tasks.

Experimental outcomes underscore the excellence of our method in managing brain tumor boundary regions. Notably, the Hausdorff distance (HD) metric reveals a significant reduction when compared to traditional methods, attaining values of 1.82, 1.31, and 2.30 across the three datasets, respectively. Furthermore, our method demonstrates strong performance in handling feature information, successfully mitigating common issues related to edge blurring and indistinct segmentation in brain tumor segmentation. The robustness of our method is consistently validated across diverse datasets. To address data imbalance concerns, we incorporate the Focal Tversky loss function, providing additional guidance for the segmentation model. Through meticulous hyperparameter tuning and improvements to the model loss function, we achieve enhanced stability in segmentation outcomes.

5. Conclusions

The main objective of this paper is to accurately partition 2D brain tumor images with the U-Net network. We leverage the inherent advantages of the U-Net network's fundamental structure while deepening its architecture with the incorporation of VGG19. This modification allows for the extraction of deep features from input brain tumor images using smaller convolutional kernels. Furthermore, we propose the incorporation of the convolutional attention mechanism module for the purpose of computing feature scores and extracting global information. This, in turn, enhances the accuracy of model training by filtering out irrelevant noise information while emphasizing key details.

Additionally, we address the challenge of predicting unclear tumor edges, smoothing surrounding tissues, and preserving edge details by introducing an edge enhancement module. This module leverages edge detection methods to strengthen edge information, thereby alleviating difficulties in medical segmentation. The feasibility of the method is proved by experiments, and the model exhibits strong performance on the given dataset.

In subsequent endeavors, our intention is to investigate the potential use of the methodology put out in this scholarly article for the examination of 3D brain tumor images. This direction aims to overcome the limitation of 2D convolutional networks, which

may not capture the full extent of 3D spatial information. Our research will focus on developing and adapting techniques that can effectively process and extract relevant features from 3D medical imaging data.

CRediT authorship contribution statement

Dapeng Cheng: Data curation, Formal analysis. **Xiaolian Gao:** Conceptualization, Data curation, Formal analysis, Investigation, Methodology, Resources, Software, Validation, Visualization, Writing – original draft, Writing – review & editing. **Yanyan Mao:** Data curation, Formal analysis. **Baozhen Xiao:** Data curation, Formal analysis. **Panlu You:** Data curation. **Jiale Gai:** Data curation. **Minghui Zhu:** Data curation. **Jialong Kang:** Data curation. **Feng Zhao:** Data curation. **Ning Mao:** Data curation.

Declaration of competing interest

The authors declare the following financial interests/personal relationships which may be considered as potential competing interests:

Dapeng Cheng reports financial support was provided by Foundation for Innovative Research Groups of the National Natural Science Foundation of China.

Data availability

The data that support the findings of this study are openly available in LGG Segmentation Dataset at https://doi.org/10.1016/j.compbiomed.2019.05.002 brain tumor dataset at https://doi.org/10.6084/m9.figshare.1512427.v5, and BraTS2021 at https://doi.org/10.48550/arXiv.2107.02314 reference number [36–38].

Acknowledgement

This work was supported in part by the National Natural Science Foundation of China (62176140).

References

[1] Y. Chen, J. Joo, Understanding and mitigating annotation bias in facial expression recognition, in: Proceedings of the IEEE/CVF International Conference on Computer Vision, 2021, pp. 14980–14991.
[2] Y. Cui, M. Jia, T.-Y. Lin, Y. Song, S. Belongie, Class-balanced loss based on effective number of samples, in: Proceedings of the IEEE/CVF Conference on Computer Vision and Pattern Recognition, 2019, pp. 9268–9277.
[3] T. Jemimma, Y.J. Vetharaj, A survey on brain tumor segmentation and classification, Int. J. Softw. Innov. (IJSI) 10 (1) (2022) 1–21, https://doi.org/10.4018/IJSI.309721.
[4] S. Rota Bulo, G. Neuhold, P. Kontschieder, Loss max-pooling for semantic image segmentation, in: Proceedings of the IEEE Conference on Computer Vision and Pattern Recognition, 2017, pp. 2126–2135.
[5] Z. Liu, L. Tong, L. Chen, Z. Jiang, F. Zhou, Q. Zhang, X. Zhang, Y. Jin, H. Zhou, Deep learning based brain tumor segmentation: a survey, Complex Intell. Syst. 9 (1) (2023) 1001–1026, https://doi.org/10.1007/s40747-022-00815-5.
[6] X. Ding, X. Zhang, J. Han, G. Ding, Scaling up your kernels to 31x31: revisiting large kernel design in CNNs, in: Proceedings of the IEEE/CVF Conference on Computer Vision and Pattern Recognition, 2022, pp. 11963–11975.
[7] L. ZongRen, W. Silamu, W. Yuzhen, W. Zhe, DenseTrans: multimodal brain tumor segmentation using swin transformer, IEEE Access 11 (2023) 42895–42908, https://doi.org/10.1109/ACCESS.2023.3272055.
[8] Z. Tao, C. XiaoYu, L. HuiLing, Y. XinYu, L. YunCan, Z. XiaoMin, Pooling operations in deep learning: from "invariable" to "variable", BioMed Res. Int. 2022 (2022), https://doi.org/10.1155/2022/4067581.
[9] X. Ding, X. Zhang, N. Ma, J. Han, G. Ding, J. Sun, RepVGG: making VGG-style ConvNets great again, in: 2021 IEEE/CVF Conference on Computer Vision and Pattern Recognition (CVPR), 2021, pp. 13728–13737.
[10] S. Mascarenhas, M. Agarwal, A comparison between VGG16, VGG19 and ResNet50 architecture frameworks for image classification, in: 2021 International Conference on Disruptive Technologies for Multi-Disciplinary Research and Applications (CENTCON), vol. 1, IEEE, 2021, pp. 96–99.
[11] D. Sarwinda, R.H. Paradisa, A. Bustamam, P. Anggia, Deep learning in image classification using residual network (ResNet) variants for detection of colorectal cancer, Proc. Comput. Sci. 179 (2021) 423–431, https://doi.org/10.1016/j.procs.2021.01.025.
[12] A. Deshpande, V.V. Estrela, P. Patavardhan, The DCT-CNN-Resnet50 architecture to classify brain tumors with super-resolution, convolutional neural network, and the ResNet50, Neurosci. Inf. 1 (4) (2021) 100013, https://doi.org/10.1016/j.neuri.2021.100013.
[13] T. Zhou, Q. Li, H. Lu, Q. Cheng, X. Zhang, Gan review: models and medical image fusion applications, Inf. Fusion 91 (2023) 134–148, https://doi.org/10.1016/j.inffus.2022.10.017.
[14] Z. Akkus, A. Galimzianova, A. Hoogi, D.L. Rubin, B.J. Erickson, Deep learning for brain MRI segmentation: state of the art and future directions, J. Digit. Imag. 30 (2017) 449–459, https://doi.org/10.1007/s10278-017-9983-4.
[15] S. Gull, S. Akbar, Artificial intelligence in brain tumor detection through MRI scans: advancements and challenges, in: Artificial Intelligence and Internet of Things, 2021, pp. 241–276.
[16] A. Tiwari, S. Srivastava, M. Pant, Brain tumor segmentation and classification from magnetic resonance images: review of selected methods from 2014 to 2019, Pattern Recognit. Lett. 131 (2020) 244–260, https://doi.org/10.1016/j.patrec.2019.11.020.
[17] X. Zhao, Y. Wu, G. Song, Z. Li, Y. Zhang, Y. Fan, A deep learning model integrating FCNNs and CRFs for brain tumor segmentation, Med. Image Anal. 43 (2018) 98–111, https://doi.org/10.1016/j.media.2017.10.002.
[18] O. Ronneberger, P. Fischer, T. Brox, U-Net: convolutional networks for biomedical image segmentation, in: Medical Image Computing and Computer-Assisted Intervention–MICCAI 2015: 18th International Conference, Proceedings, Part III, Munich, Germany, October 5–9, 2015, vol. 18, Springer, 2015, pp. 234–241.
[19] J. Long, E. Shelhamer, T. Darrell, Fully convolutional networks for semantic segmentation, in: Proceedings of the IEEE Conference on Computer Vision and Pattern Recognition, 2015, pp. 3431–3440.

[20] Y. Fu, G. Zhang, X. Lu, H. Wu, D. Zhang, RMCA U-net: hard exudates segmentation for retinal fundus images, Expert Syst. Appl. 234 (2023) 120987, https://doi.org/10.1016/j.eswa.2023.120987.
[21] R. Brügger, C.F. Baumgartner, E. Konukoglu, A partially reversible U-Net for memory-efficient volumetric image segmentation, in: Medical Image Computing and Computer Assisted Intervention–MICCAI 2019: 22nd International Conference, Proceedings, Part III, Shenzhen, China, October 13–17, 2019, vol. 22, Springer, 2019, pp. 429–437.
[22] Y. Hao, H. Jiang, Z. Diao, T. Shi, L. Liu, H. Li, W. Zhang, Msu-net: multi-scale sensitive U-Net based on pixel-edge-region level collaborative loss for nasopharyngeal MRI segmentation, Comput. Biol. Med. 159 (2023) 106956, https://doi.org/10.1016/j.compbiomed.2023.106956.
[23] C. Li, Y. Tan, W. Chen, X. Luo, Y. He, Y. Gao, F. Li, ANU-Net: attention-based nested U-Net to exploit full resolution features for medical image segmentation, Comput. Graph. 90 (2020) 11–20, https://doi.org/10.1016/j.cag.2020.05.003.
[24] Z. Zhou, M.M. Rahman Siddiquee, N. Tajbakhsh, J. Liang, Unet++: a nested U-Net architecture for medical image segmentation, in: Deep Learning in Medical Image Analysis and Multimodal Learning for Clinical Decision Support: 4th International Workshop, DLMIA 2018, and 8th International Workshop, Proceedings, ML-CDS 2018, Held in Conjunction with MICCAI 2018, Granada, Spain, September 20, 2018, vol. 4, Springer, 2018, pp. 3–11.
[25] H. Tang, J. Liu, M. Zhao, X. Gong, Progressive layered extraction (PLE): a novel multi-task learning (MTL) model for personalized recommendations, in: Proceedings of the 14th ACM Conference on Recommender Systems, 2020, pp. 269–278.
[26] X. Sun, R. Panda, R. Feris, K. Saenko, AdaShare: learning what to share for efficient deep multi-task learning, Adv. Neural Inf. Process. Syst. 33 (2020) 8728–8740, https://doi.org/10.48550/arXiv.1911.12423.
[27] S. Liu, E. Johns, A.J. Davison, End-to-end multi-task learning with attention, in: 2019 IEEE/CVF Conference on Computer Vision and Pattern Recognition (CVPR), 2019, pp. 1871–1880.
[28] S. Woo, J. Park, J.-Y. Lee, I.S. Kweon, CBAM: convolutional block attention module, in: Proceedings of the European Conference on Computer Vision (ECCV), 2018, pp. 3–19.
[29] H. Shen, R. Wang, J. Zhang, S.J. McKenna, Boundary-aware fully convolutional network for brain tumor segmentation, in: Medical Image Computing and Computer-Assisted Intervention - MICCAI 2017: 20th International Conference, Proceedings, Part II, Quebec City, QC, Canada, September 11–13, 2017, vol. 20, Springer, 2017, pp. 433–441.
[30] J. Sun, Q. Ge, X. Li, B. Zhao, A medical image segmentation network with boundary enhancement, J. Electron. Inf. Technol. 44 (5) (2022) 1643–1652, https://doi.org/10.11999/JEIT210784.
[31] D. Sharifrazi, R. Alizadehsani, M. Roshanzamir, J.H. Joloudari, A. Shoeibi, M. Jafari, S. Hussain, Z.A. Sani, F. Hasanzadeh, F. Khozeimeh, et al., Fusion of convolution neural network, support vector machine and Sobel filter for accurate detection of COVID-19 patients using X-ray images, Biomed. Signal Process. Control 68 (2021) 102622, https://doi.org/10.48550/arXiv.2102.06883.
[32] Z. Zhang, M. Sabuncu, Generalized cross entropy loss for training deep neural networks with noisy labels, Adv. Neural Inf. Process. Syst. 31 (2018), https://doi.org/10.48550/arXiv.1805.07836.
[33] S.S.M. Salehi, D. Erdogmus, A. Gholipour, Tversky loss function for image segmentation using 3D fully convolutional deep networks, in: Machine Learning in Medical Imaging: 8th International Workshop, Proceedings, MLMI 2017, Held in Conjunction with MICCAI 2017, Quebec City, QC, Canada, September 10, 2017, vol. 8, Springer, 2017, pp. 379–387.
[34] N. Abraham, N.M. Khan, A novel focal Tversky loss function with improved attention U-Net for lesion segmentation, in: 2019 IEEE 16th International Symposium on Biomedical Imaging (ISBI 2019), 2019, pp. 683–687.
[35] The cancer genome atlas program (TCGA), [EB/OL], https://cancergenome.nih.gov/cancersselected/lowergradeglioma. (Accessed 20 January 2023).
[36] M. Buda, A. Saha, M.A. Mazurowski, Association of genomic subtypes of lower-grade gliomas with shape features automatically extracted by a deep learning algorithm, Comput. Biol. Med. 109 (2019) 218–225, https://doi.org/10.1016/j.compbiomed.2019.05.002.
[37] J. Cheng, Brain tumor dataset (4 2017), https://doi.org/10.6084/m9.figshare.1512427.v5, https://figshare.com/articles/dataset/brain_tumor_dataset/1512427.
[38] U. Baid, S. Ghodasara, S. Mohan, M. Bilello, E. Calabrese, E. Colak, K. Farahani, J. Kalpathy-Cramer, F.C. Kitamura, S. Pati, et al., The RSNA-ASNR-MICCAI BraTS 2021 benchmark on brain tumor segmentation and radiogenomic classification, arXiv preprint, arXiv:2107.02314, 2021, https://doi.org/10.48550/arXiv.2107.02314.